

## Symmetry analysis and uniaxial-stress effect on the low-field electroreflectance of Si from 3.0 to 4.0 eV

K. Kondo and A. Moritani

*Department of Electronics, Faculty of Engineering, Osaka University, Suita, Osaka, Japan*

(Received 29 December 1975)

The low-field electroreflectance (ER) spectra of Si in the energy range from 3.0 to 4.0 eV have been measured and analyzed in the absence and in the presence of strain. In the absence of strain, the symmetry location  $\vec{K}_0$  of a critical point can be deduced from both the polarization anisotropies and the line shape of a low-field ER spectrum. Uniaxial-stress effects on a low-field ER spectrum are also described in the low-strain limit. These results are used to reveal the 3.4-eV complexities. The structures of the low-field ER spectrum of Si from 3.0 to 4.0 eV may arise from two critical points with different symmetries. First, the main structure in the higher-energy side is attributed conclusively to a high-symmetry critical point along the  $\Lambda$  axis (or at the  $L$  point) in the Brillouin zone [ $\Lambda_3^v \rightarrow \Lambda_1^c$  (or  $L_3^v \rightarrow L_1^c$ ) in Si]. The experimentally determined band-edge parameters are as follows: the critical-point energy  $E_g = 3.412 \pm 0.005$  eV (300 K); the phenomenological broadening energy  $\Gamma = 0.060 \pm 0.005$  eV (300 K); and the pair band deformation-potential parameters  $D_1^c = -9.8 \pm 1.3$  eV,  $D_1^v = 6.5 \pm 1.4$  eV,  $\mathfrak{D}_3^c = 4.7 \pm 0.5$  eV, and  $\mathfrak{D}_3^v = 3.0 \pm 1.7$  eV (77 K). In addition, this critical point is three-dimensional  $M_1$  type and the relations between the assumed reduced masses  $\mu_T$  and  $\mu_L$  are  $\mu_T \ll |\mu_L|$ ,  $\mu_T > 0$ , and  $\mu_L < 0$ . From the mass relation,  $\mu_T \ll |\mu_L|$ , the critical point may be nearly two-dimensional ( $M_0$  type). Second, for the weak structure in the lower-energy side the experimental results under uniaxial stress can not be explained by any high-symmetry critical point except the degenerate critical point in the  $\Delta$  direction ( $\Delta_2^v \rightarrow \Delta_1^c$  near  $\Gamma$  in Si). If we assume that this structure is attributed to the  $\Delta$  critical point, the experimentally determined parameters are as follows:  $E_g = 3.294 \pm 0.005$  eV (300 K);  $\Gamma = 0.060 \pm 0.005$  eV (300 K); and this critical point is three-dimensional  $M_0$  type ( $\mu_T/\mu_L = 1-3$ ).

### I. INTRODUCTION

It is very useful to obtain detailed information about the optical-critical-point structures in order to study the energy-band structures of solids. In particular, the energy  $E_g$ , the location  $\vec{K}_0$  in the Brillouin zone (BZ), and the relation between the assumed reduced masses of a critical point are essential in describing the  $E(\vec{k} - \vec{K}_0)$  topology of interband energy surfaces.

Since the introduction of electroreflectance (ER) technique by Seraphin,<sup>1</sup> various types of differential methods<sup>2, 3</sup> have been devised and applied to make clear the optical-critical-point structures of semiconductors. In recent years, it has been shown by Aspnes<sup>4, 5</sup> that the low-field ER technique is suitable for the precise study of energy-band structures, since this technique provides spectra concerned directly with high-symmetry critical points: A low-field ER spectrum is described by the highly resonant function (the third derivative of the unperturbed dielectric function  $\epsilon$ ) in the vicinity of a critical point. Values of band-edge parameters, such as the energy  $E_g$ , the phenomenological broadening energy  $\Gamma$ , and the type of a critical point, may be obtained from the best-fit analysis on low-field ER line shapes.<sup>5</sup> Symmetry information about the location  $\vec{K}_0$  of the related critical point may also be obtained from low-field ER spectra.<sup>6, 7</sup>

It is the purpose of this paper to describe a symmetry analysis and uniaxial-stress effects on a low-field ER spectrum and apply them to Si. The location  $\vec{K}_0$  of a critical point can be determined from the polarization anisotropies and the line shapes of a low-field ER spectrum. From these two observations it may also be possible to obtain the reduced-mass relations at a critical point. Moreover, it is clear that the symmetry-breaking perturbation of uniaxial stress is useful for the symmetry study of critical-point structures. Polak and Cardona<sup>8</sup> have combined this perturbation with ER technique for the first time, in order to study Ge, GaAs, and Si using the electrolyte configuration. Their analysis on the ER spectra of Si, however, was insufficient in the sense that the spectra under uniaxial stress were measured out of the low-field conditions and quantitative comparison with the ER theory was unsatisfactory. We show the results of uniaxial-stress effects using the Schottky-barrier ER technique. The availability of the Schottky-barrier ER technique has been described in detail by Aspnes.<sup>7</sup> In addition, this technique is advantageous for applying static uniaxial stress, because the evaporated metal on a semiconductor surface may remain in uniform contact with it when the sample is elastically deformed by the stress. The stress effects observed in a low-field ER spectrum may be analyzed according to Kane's theory of piezore-

flectance.<sup>9</sup>

In this paper, we shall concentrate on the 3.4-eV optical structures of Si in order to reveal its complexities. The 3.4-eV optical structures have been the subject of controversy for a long time. A number of experimental and theoretical investigations in this energy region have been performed as outlined by Pollak and Rubloff.<sup>10</sup> As for the ER measurements of Si, the pioneering work has been made in the MIS (metal-insulator-semiconductor) configuration by Seraphin<sup>11</sup>; later works have followed in the electrolyte<sup>12-14</sup> and in the transverse-electric-field<sup>15</sup> configurations. Most of the results suggest that the 3.4-eV optical structures arise from at least two distinct critical points with different symmetries. For assignment of the main structure, however, both experimental and theoretical evidence may be divided into two parts: the  $\Lambda_3^v - \Lambda_1^c$  transition<sup>10, 16-22</sup> and  $\Delta_5^v - \Delta_1^c$  transition near the  $\Gamma$  point (including the  $\Gamma_{25}^v - \Gamma_{15}^c$  transition).<sup>8, 23-33</sup> Recent experiments support the  $\Lambda$  assignment.<sup>10, 34</sup> On the other hand, the existence of an extremely complex nest of critical points in this energy region has been predicted from detailed band-structure calculations.<sup>21, 33, 35, 36</sup> Saravia and Brust<sup>35</sup> have shown that the 3.4-eV structures of  $\epsilon_2$  come mainly from two regions near the  $\Gamma$  point and  $\Lambda$  line (including the  $L$  point) and that the relative position of the  $\Gamma_{25}^v - \Gamma_{15}^c$  and  $L_3^v - L_1^c$  transitions in energy affect the shape of  $\epsilon_2$ .

The outline of this paper is as follows: In Sec. II A, a method of symmetry analysis of a low-field ER spectrum is described; polarization dependences of a longitudinal ER spectrum on the  $(1\bar{1}0)$  face are listed in Table I for high-symmetry  $\Gamma$ ,  $\Delta$ ,  $\Lambda(L)$ , and  $\Sigma$  critical points in diamond-type crystals with criteria for determining the location  $\bar{K}_0$  in the BZ. Uniaxial-stress effects on a low-field ER spectrum are discussed in Sec. II B; and the results for the degenerate  $\Lambda_3^v - \Lambda_1^c$  (or  $L_3^v - L_1^c$ ) and  $\Delta_5^v - \Delta_1^c$  critical points are summarized in Tables II and III, respectively. In Sec. III, experimental details of sample preparation, measurement techniques, and stress arrangement are described. The data are presented and analyzed in Sec. IV. Finally, in Sec. V we compare our results to other measurements and calculations of the energy-band parameters of Si.

## II. SYMMETRY ANALYSIS

### A. In the absence of strain

A theoretical basis for ER symmetry analysis has been reviewed by Seraphin<sup>37</sup> and later by Rehn.<sup>6</sup> In this section, we describe a method of symmetry analysis on a low-field ER spectrum in diamond-

type crystals. At sufficiently low fields, the ER spectrum can be represented with terms varying linearly (linear ER) and quadratically (quadratic ER) with electric field.<sup>4</sup> In diamond-type crystals, there is only the quadratic term and the linear term becomes zero due to inversion symmetry. The quadratic term may be factored into line-shape and symmetry parts if we make several assumptions: The optical matrix element is  $\bar{k}$  independent and the applied electric field is small enough not to change the selection rules of the transition. Following Aspnes,<sup>5</sup> the relative reflectivity change  $\Delta R/R$ , measured in a low-field ER experiment, is given by

$$\frac{\Delta R}{R}(\hbar\omega + i\Gamma) = \text{Re} \left\{ \bar{C} [\alpha(\hbar\omega) - i\beta(\hbar\omega)] i^{l-3} \times L(\hbar\omega + i\Gamma) \right\} \mathcal{E}^2 F, \quad (2.1a)$$

where

$$F = \sum_{\nu, \alpha} \sum_{i, j, u, v} n_i^\nu n_j^\nu P_i^\alpha P_j^\alpha \mathcal{E}_u^\nu \mathcal{E}_v^\nu \mu_{uv}^{-1}, \quad (2.1b)$$

$$\mu_{uv}^{-1} = \frac{1}{\hbar^2} \frac{\partial^2}{\partial k_u \partial k_v} E(\bar{k} - \bar{K}_0), \quad (2.1c)$$

$$P_i^\alpha = \langle 0 | p_i | \psi_\alpha \rangle. \quad (2.1d)$$

$\text{Re} \{ \}$  and  $\mathcal{E}^2 F$  give the line-shape and the symmetry parts, respectively. In the line-shape part,  $\bar{C}$  is the product of complex functions which represent the effect of a nonuniform modulating field<sup>38</sup> and the electron-hole effect in the contact exciton approximation.<sup>39</sup> The function  $[\alpha(\hbar\omega) - i\beta(\hbar\omega)]$  is the complex Seraphin coefficient.<sup>37</sup> The function  $i^{l-3} L(\hbar\omega + i\Gamma)$  mainly determines the line shape of an ER spectrum. One-, two-, and three-dimensional forms of  $L(\hbar\omega + i\Gamma)$  are summarized in Ref. 4. We can use these functions for the best-fit analysis on the experimentally obtained low-field ER line shapes. In addition,  $l$  is the number of negative reduced masses at a critical point, which is said to be of type  $M_l$  ( $l=0, 1, 2, 3$ ); this number produces four typical line shapes of a low-field ER spectrum for the three-dimensional critical point. The symmetry part represents the effects of polarization and applied electric field on a low-field ER spectrum, which determines polarization anisotropies of the spectrum. This factor is written in detail in the form of Eq. (2.1b), where  $\hat{n}$  is the unit polarization vector of the incident light.  $P$  is the optical matrix element of the momentum operator between the ground state  $|0\rangle$  and the excited state  $|\psi\rangle$ , which may be written in the form of Eq. (2.1d) if dipole interaction is assumed.  $\hat{\mathcal{E}}$  is the unit vector of the applied electric field;  $\mathcal{E}$  is its magnitude.  $\mu_{uv}$  is the component of the second-rank interband

reduced-mass tensor, which is defined in Eq. (2.1c).  $\sum_{\alpha}$  represents the sum over the order of degeneracy of a critical point.  $\sum_{\nu}$  represents the sum over all the equivalent critical-point set, in which the superscript  $\nu$  of  $\hat{n}$  or  $\hat{\mathcal{G}}$  shows that it is the effective component at the  $\nu$ th equivalent critical point.  $\sum_{i, j, u, \nu}$  shows the sum over the cubic components.

We wish to describe the ER form factor  $F$  in a more convenient form for high-symmetry  $\Gamma, \Delta, \Lambda (L)$ , and  $\Sigma$  critical points in diamond-type crystals. The  $X$  point may not be a critical point because of its  $\vec{k} - \vec{K}_0$  linear term. We treat the case that the effect of spin-orbit interaction is negligibly small compared to the effect of lifetime broadening. First, the  $\vec{k}$  dependence of the interband energy in the vicinity of a high-symmetry critical point may be written in a parabolic form, using the three principal reduced-mass parameters  $\mu_{T_1}$ ,  $\mu_{T_2}$ , and  $\mu_L$ :

$$E(\vec{k} - \vec{K}_0) \cong E_{\varepsilon} + \frac{\hbar^2 k_{T_1}^2}{2\mu_{T_1}} + \frac{\hbar^2 k_{T_2}^2}{2\mu_{T_2}} + \frac{\hbar^2 k_L^2}{2\mu_L}, \quad (2.2)$$

where  $k_{T_1}$ ,  $k_{T_2}$ , and  $k_L$  are the three principal axes of the  $\vec{k} - \vec{K}_0$  space, in which the longitudinal axis  $k_L$  is defined to be parallel to the representative vector  $\vec{K}_0$  of the critical point. Moreover, we assume local rotational symmetry around  $\vec{K}_0$  for the  $\Delta$  or  $\Lambda$  (or  $L$ ) critical point; whence the interband reduced-mass tensor has two  $\vec{k}$ -independent diagonal components  $\mu_T$  ( $\equiv \mu_{T_1} = \mu_{T_2}$ ) and  $\mu_L$ . For the  $\Gamma$  critical point, we assume spherical symmetry; then the reduced-mass tensor has all equal diagonal components  $\mu$  ( $\equiv \mu_{T_1} = \mu_{T_2} = \mu_L$ ). These simple parabolic models of the effective-mass approximation enable us to treat the transition between degenerate bands as the sum of transitions between nondegenerate bands. This assumption seems to be oversimplified and it is probably accepted only in the case of optical transitions with large broadening energy; the effect of band degeneracy, such as band warping, may be neglected in the low-field modulation limit. Second, according to Kane,<sup>9</sup> optical critical points along (or at) the high-symmetry axes (or points) in the BZ may be represented by the irreducible pair states which transform in the same way as the irreducible components of the momentum operator under the group of  $\vec{K}_0$ , when only the excited states which couple strongly to light are taken into consideration. Therefore, the ER form factor  $F$  of Eq. (2.1b) may be written

$$F = \sum_{\nu, \alpha} (\hat{n}^{\nu} \cdot \hat{B}_{\gamma\alpha})^2 \left( \frac{(\mathcal{G}_{T_1}^{\nu})^2}{\mu_{T_1}} + \frac{(\mathcal{G}_{T_2}^{\nu})^2}{\mu_{T_2}} + \frac{(\mathcal{G}_L^{\nu})^2}{\mu_L} \right) f^0, \quad (2.3)$$

$$f^0 \equiv \langle 0 | p_{\gamma\alpha} | \psi_{\gamma\alpha} \rangle^2, \quad (2.4)$$

where  $\hat{B}_{\gamma\alpha}$  is the unit vector transforming in the same way as the pair state ( $\psi_{\gamma\alpha}$ ) with symmetry  $U_{\gamma}$  under the group of  $\vec{K}_0$ :  $\hat{B}_{4x} = (1, 0, 0)$ ,  $\hat{B}_{4y} = (0, 1, 0)$ , and  $\hat{B}_{4z} = (0, 0, 1)$  for the  $\Gamma$  critical point with symmetry  $U_{4-}$ ;  $\hat{B}_1 = (0, 0, 1)$  for the  $\Delta$  critical point with symmetry  $U_1$ , and  $\hat{B}_{5T_1} = (1, 0, 0)$  and  $\hat{B}_{5T_2} = (0, 1, 0)$  for the  $\Delta$  critical point with symmetry  $U_5$ ;  $\hat{B}_1 = (1/\sqrt{3}, 1/\sqrt{3}, 1/\sqrt{3})$  for the  $\Lambda$  critical point with symmetry  $U_1$ ,  $\hat{B}_{3T_1} = (1/\sqrt{2}, -1/\sqrt{2}, 0)$  and  $\hat{B}_{3T_2} = (1/\sqrt{6}, 1/\sqrt{6}, -2/\sqrt{6})$  for the  $\Lambda$  critical point with symmetry  $U_3$ ;  $\hat{B}_1 = (1/\sqrt{2}, 1/\sqrt{2}, 0)$  for the  $\Sigma$  critical point with symmetry  $U_1$ ,  $\hat{B}_2 = (0, 0, 1)$  for the  $\Sigma$  critical point with symmetry  $U_2$ , and  $\hat{B}_3 = (1/\sqrt{2}, -1/\sqrt{2}, 0)$  for the  $\Sigma$  critical point with symmetry  $U_3$ .  $\mathcal{G}_{T_1}$ ,  $\mathcal{G}_{T_2}$ , and  $\mathcal{G}_L$  are defined in the same form as the three principal axes  $k_{T_1}$ ,  $k_{T_2}$ , and  $k_L$ , respectively.  $f^0$  is a unit of the ER form factor defined in Eq. (2.4).

We will consider only a longitudinal ER geometry in order to analyze the Schottky-barrier ER spectra, in which the direction of the incident light and the modulation field are normal to the plane of reflection. Moreover, we will choose the  $(1\bar{1}0)$  face for the plane of reflection, since this surface includes all four high-symmetry directions ( $[001]$ ,  $[11\bar{2}]$ ,  $[111]$ , and  $[110]$ ) obtained in diamond-type crystals. For  $\Delta$ ,  $\Lambda$  (or  $L$ ), and  $\Sigma$  critical points, we sum over the star of  $\vec{K}_0$  by summing over the effective components of  $\hat{n}^{\nu}$  and  $\hat{\mathcal{G}}^{\nu}$  in Eq. (2.3).<sup>40</sup> The polarization dependences of the ER form factor on the  $(1\bar{1}0)$  face in the low-field modulation limit are listed in Table I. In Table I, we also list conditions on the polarization anisotropy  $r \equiv F_{[001]}/F_{[110]}$  (or  $s \equiv F_{[111]}/F_{[11\bar{2}]}$ ) for all types of critical point, which may be used as criteria of symmetry analysis combined with the type of critical point determined from the line-shape analysis. In the case that the effect of spin-orbit interaction is large compared to the lifetime broadening, polarization dependences of the two split-off structures in a low-field ER spectrum may also be calculated. The results are the same as listed in Table I for each of the two split-off structures.

This method of symmetry analysis, however, cannot lead us to the unique conclusion in some cases, since the conditions for some critical points listed in Table I are not exclusive of each other. We can get rid of this difficulty with help of the results of band-structure calculations. Moreover, the three-dimensional ER line shapes of  $M_{1\perp}$  and  $M_{1\parallel}$ , or  $M_{2\parallel}$  and  $M_{2\perp}$  critical points may not be distinguished from each other in the low-field modulation limit or in the large broadening region. It may be useful to measure ER spectra

TABLE I. Polarization dependences of a low-field electroreflectance form factor  $F$  for  $\Gamma$ ,  $\Delta$ ,  $\Lambda$  ( $L$ ), and  $\Sigma$  critical points in diamond-type crystals. A longitudinal geometry is used and (110) face is preferred for the plane of reflection; the electric field  $\vec{\mathcal{E}} = (1/\sqrt{2}, -1/\sqrt{2}, 0)$ .  $\theta$  is the polarization angle of the incident light measured with respect to the crystallographic  $\hat{z}$  direction. The polarization anisotropy is defined as  $r \equiv F_{[001]}/F_{[110]}$  (or  $s \equiv F_{[111]}/F_{[1\bar{1}\bar{2}]}$ ); the subscript of  $F$  denotes the polarization of the incident light.

Critical-point location	Pair state symmetry	Polarization dependences of a low-field electroreflectance form factor $F$	Conditions of the polarization anisotropy $r$ (or $s$ ) for all types of a critical point
$\Gamma$	$U_{4-}$	$(1/\mu)f^0$	for all cases; $M_0, M_3$
$\Delta$	$U_1$	$\frac{1}{2} \left[ \left( \frac{3}{\mu_T} + \frac{1}{\mu_L} \right) + \left( \frac{1}{\mu_T} - \frac{1}{\mu_L} \right) \cos 2\theta \right] f^0$	$0 \leq r \leq 2$ ( $\frac{4}{5} \leq s \leq 2$ ); $M_0, M_3$ $r \leq 0, 2 \leq r$ ( $s \leq \frac{4}{5}, 2 \leq s$ ); $M_1, M_2$
	$U_5$	$\frac{1}{2} \left[ \left( \frac{5}{\mu_T} + \frac{3}{\mu_L} \right) - \left( \frac{1}{\mu_T} - \frac{1}{\mu_L} \right) \cos 2\theta \right] f^0$	$\frac{2}{3} \leq r \leq 2$ ( $\frac{4}{5} \leq s \leq \frac{8}{7}$ ); $M_0, M_3$ $r \leq \frac{2}{3}, 2 \leq r$ ( $s \leq \frac{4}{5}, \frac{8}{7} \leq s$ ); $M_1, M_2$
$\Lambda$ ( $L$ )	$U_1$ ( $U_{2-}$ )	$\frac{4}{9} \left[ \left( \frac{5}{\mu_T} + \frac{1}{\mu_L} \right) - \left( \frac{1}{\mu_T} - \frac{1}{\mu_L} \right) \cos 2\theta \right] f^0$	$\frac{2}{3} \leq r$ ( $\frac{1}{2} \leq s \leq \frac{8}{7}$ ); $M_0, M_3$ $r \leq \frac{2}{3}$ ( $s \leq \frac{1}{2}, \frac{8}{7} \leq s$ ); $M_1, M_2$
	$U_3$ ( $U_{3-}$ )	$\frac{4}{9} \left[ \left( \frac{7}{\mu_T} + \frac{5}{\mu_L} \right) + \left( \frac{1}{\mu_T} - \frac{1}{\mu_L} \right) \cos 2\theta \right] f^0$	$\frac{2}{3} \leq r \leq \frac{4}{3}$ ( $\frac{10}{11} \leq s \leq \frac{8}{7}$ ); $M_0, M_3$ $r \leq \frac{2}{3}, \frac{4}{3} \leq r$ ( $s \leq \frac{10}{11}, \frac{8}{7} \leq s$ ); $M_1, M_2$
$\Sigma$	$U_1$	$\frac{1}{4} \left[ \left( \frac{2}{\mu_{T1}} + \frac{1}{\mu_L} \right) (3 + 2\sqrt{2} \sin 2\theta + \cos 2\theta) \right. \\ \left. + \left( \frac{1}{\mu_{T2}} \right) (7 + 2\sqrt{2} \sin 2\theta - 3 \cos 2\theta) \right] f^0$	$\frac{2}{5} \leq r \leq 2$ ; $\left( \frac{2}{\mu_{T1}} + \frac{1}{\mu_L} \right) \frac{1}{\mu_{T2}} \geq 0$ ( $\frac{4}{5} \leq s \leq \frac{4}{3}$ )
	$U_2$	$\frac{1}{2} \left[ \frac{2}{\mu_{T1}} (1 - \cos 2\theta) + \left( \frac{1}{\mu_{T2}} + \frac{1}{\mu_L} \right) \right. \\ \left. \times (3 + \cos 2\theta) \right] f^0$	$0 \leq r \leq 2$ ; $\left( \frac{1}{\mu_{T2}} + \frac{1}{\mu_L} \right) \frac{1}{\mu_{T1}} \geq 0$ ( $\frac{4}{5} \leq s \leq 2$ )
	$U_3$	$\frac{1}{4} \left[ \left( \frac{2}{\mu_{T1}} + \frac{1}{\mu_{T2}} \right) (3 - 2\sqrt{2} \sin 2\theta + \cos 2\theta) \right. \\ \left. + \left( \frac{1}{\mu_L} \right) (7 - 2\sqrt{2} \sin 2\theta - 3 \cos 2\theta) \right] f^0$	$\frac{2}{5} \leq r \leq 2$ ; $\left( \frac{2}{\mu_{T1}} + \frac{1}{\mu_{T2}} \right) \frac{1}{\mu_L} \geq 0$ ( $\frac{4}{5} \leq s \leq \frac{4}{3}$ )
			$r \leq \frac{2}{5}, 2 \leq r$ ; $\left( \frac{2}{\mu_{T1}} + \frac{1}{\mu_{T2}} \right) \frac{1}{\mu_L} \leq 0$ ( $s \leq \frac{4}{5}, \frac{4}{3} \leq s$ )

in the Franz-Keldysh range in order to determine the type of critical point correctly.

#### B. In the presence of strain

The application of a uniaxial stress and the related strain produces a change in the lattice parameter and the symmetry of solids, which results in significant changes in the electronic band structures, such as shifts of energy levels<sup>41-44</sup> and mixing of wave functions.<sup>8,9</sup> Considering optical transitions, strain induces changes of the interband energy  $E(\vec{k} - \vec{k}_0)$  and variations of the optical matrix element  $P$  including the selection rules. These changes would be observed in the structures of a low-field ER spectrum as (i) energy shifts

and splittings, (ii) dependences on polarization, electric field direction, and stress configuration, and (iii) amplitude changes with strain. The stress effects on the low-field ER spectrum may easily be treated theoretically, when the stress applied to a solid is small enough and we can assume that the  $\vec{k}$  dependence of the interband energy  $E(\vec{k} - \vec{k}_0)$  in the vicinity of a critical point is still described in the parabolic model shown in Eq. (2.2). In this stress region, a low-field ER spectrum may be factored into line-shape and symmetry parts in the same form as shown in Eq. (2.1a) even in the presence of strain. In addition, we consider the stress effects in the linear-response region. Thus, we can calculate the stress-induced changes in the line-shape part (the energy shifts and split-

tings) and in the symmetry part (the stress-dependences of the ER form factor  $F$ ) using the effective strain Hamiltonian and the pair wave functions to first order in the strain defined by Kane.<sup>9</sup> These treatments may be accepted when the phenomenological broadening energy is large compared to the stress-induced energy shifts; in higher band transitions, the shifts are nearly always small compared to the broadening energy even for large stress.

As a specific case we will show the stress effects for the degenerate  $\Lambda_3^v - \Lambda_1^c$  (or  $L_3^v - L_1^c$ ) critical point. The optical properties of this critical point are represented by the  $U_3$  (or  $U_{3-}$ ) pair band in the  $\Lambda$  direction (or at the  $L$  point). On the other hand, the  $\Lambda$  critical point is contributed by the eight equivalent components along the  $\langle 111 \rangle$  lines in the BZ. Since uniaxial stress does not remove the inversion symmetry of the crystal, we need not consider all eight components but four along the  $[111]$ ,  $[\bar{1}\bar{1}\bar{1}]$ ,  $[\bar{1}\bar{1}1]$ , and  $[\bar{1}1\bar{1}]$  lines. We sum over the effects of these four equivalent components. The results for stresses along the  $[001]$  and  $[111]$  directions are presented in Table II, where the factor  $F$  is given for polarizations along the  $[100]$ ,  $[010]$ ,  $[001]$ ,  $[1\bar{1}0]$ , and  $[110]$  directions with  $[001]$  stress and for polarizations along the  $[1\bar{1}0]$ ,  $[11\bar{2}]$ , and  $[111]$  directions with  $[111]$  stress. In Table II,  $s_{11}$ ,  $s_{12}$ , and  $s_{44}$  are the elastic compliance constants.  $T$  is the magnitude of the applied stress  $\bar{T}$ ; its sign is minus for compression. The  $D$ 's and  $\mathfrak{D}$ 's are "band-edge" deformation-potential parameters; in detail,  $D_1^1$  is the hydrostatic parameter,  $D_1^5$  is the interband parameter for  $[111]$  stress, and  $\mathfrak{D}_3^3$  and  $\mathfrak{D}_3^5$  are the intraband parameters for  $[001]$  and  $[111]$  stresses, respectively.  $f^0$  is a unit of the ER form factor in the unstrained crystal defined by Eq. (2.4) and  $f^s$  is a change due to admixture of first-order wave function  $\psi_{3\alpha}^s$  under stress. The uniaxial-stress effects on a low-field ER spectrum for the degenerate  $\Delta_5^v - \Delta_1^c$  critical point are presented in Table III. The optical properties of this critical point are represented by the  $U_5$  pair band in the  $\Delta$  direction. In Table III,  $D_1^3$  is the interband parameter for  $[001]$  stress, and  $\mathfrak{D}_3$  and  $\mathfrak{D}_4$  are the intraband parameters for  $[001]$  and  $[111]$  stresses, respectively.  $f^s$  is a change due to admixture of first-order wave function  $\psi_{5\alpha}^s$  under stress.

### III. EXPERIMENTAL

#### A. Sample construction

The Si single-crystal samples used in the experiment were all  $n$ -type and had a room-temperature resistivity of about  $0.5 \Omega \text{ cm}$ . The epitaxial layer on  $n^+$  base was used in the measurements of ER

at room temperature. The reflecting surface of the sample is the optically flat  $(1\bar{1}0)$  face and the crystal axes on the surface were determined by cleavage lines. In the ER measurements under uniaxial stress, the single-crystal rods were used. The crystal orientation of the samples was determined from x-ray diffraction with an accuracy of 1 deg. These samples were cut into rectangular parallelepipeds to dimensions of  $12.0 \times 1.0 \times 1.0 \text{ mm}^3$  such that the long axis was in either the  $[001]$  or  $[111]$  direction. The surfaces of the samples were polished and chemically etched in order to remove surface damages. The Schottky barrier was formed on the reflecting front surface by evaporating a semitransparent Ni film. The thickness of the Ni film is estimated to be 10.0–20.0 nm from the reflectivity measurements of the Ni-Si system. A thick In film was obtained by evaporation onto the back surface of the sample in order to make a nonrectifying contact.

#### B. Measurement techniques

Electroreflectance spectra were measured with standard optical and phase-sensitive electronic detection techniques. The optical system consisted of a 500-W Ushio model UXL500D xenon lamp, a JASCO model CT-50 0.5-m grating monochromator with a 1200-line/mm grating blazed at 300 nm, a cryotip refrigerator on a cryostat in a stress apparatus, and a Hamamatsu TV model R376 photomultiplier. The polarization measurements were made with a Glan-Thompson polarizer. The samples used in the stress experiment were mounted in a sample cell of the stress apparatus such that the long axis of the sample was parallel to the pushing rod. A paper sheet was placed between the pushing rod and the top of the sample in order to reduce the effects of imperfect alignment. A static load was applied to the sample by a lever system. The dc bias and 400-Hz square-wave ac modulation voltage were applied to the metal layer by means of a thin copper wire attached to the metal film with a dot of silver paint. The detection system was as follows: The ratio  $\Delta R/R$  was measured by electronically varying the photomultiplier gain such that the dc signal of the photomultiplier, which is proportional to  $R$ , was held constant.<sup>45</sup> The ac signal of the photomultiplier by the electric field modulation, which is then a direct measure of  $\Delta R/R$ , was detected with a PAR HR-8 lock-in amplifier and recorded by a  $x-t$  recorder. We checked the observed ER spectra to be actually in the low-field modulation limit by the method shown in Ref. 5. The energy shifts of the peak positions with ac modulating field were not observed in the measurements.

TABLE II. Energy shift  $\Delta E$  and electroreflectance form factor  $F$  for the degenerate  $U_3$  band in the  $\Lambda$  direction. Spin-orbit interaction is neglected. The factor  $F$  has been summed over the eight equivalent components. The subscript of  $F$  denotes the polarization of the light.

Energy shift <sup>a</sup>	Electroreflectance form factor
	[001] stress
$\Delta E^A = \frac{D_1^1}{\sqrt{3}}(s_{11} + 2s_{12})T + \sqrt{\frac{2}{3}}\mathfrak{D}_3^3(s_{11} - s_{12})T$	$F_{[100]}^A = F_{[010]}^A = \frac{1}{4}F_{[001]}^A = \frac{4}{9}\left(\frac{2}{\mu_T} + \frac{1}{\mu_L}\right)f_+^3$
	$F_{[1\bar{1}0]}^A = \frac{4}{9}\left[\left(\frac{2}{\mu_T} + \frac{1}{\mu_L}\right) + 2\left(\frac{1}{\mu_T} - \frac{1}{\mu_L}\right)\mathcal{E}_x\mathcal{E}_y\right]f_+^3$
	$F_{[110]}^A = \frac{4}{9}\left[\left(\frac{2}{\mu_T} + \frac{1}{\mu_L}\right) - 2\left(\frac{1}{\mu_T} - \frac{1}{\mu_L}\right)\mathcal{E}_x\mathcal{E}_y\right]f_+^3$
$\Delta E^B = \frac{D_1^1}{\sqrt{3}}(s_{11} + 2s_{12})T - \sqrt{\frac{2}{3}}\mathfrak{D}_3^3(s_{11} - s_{12})T$	$F_{[100]}^B = F_{[010]}^B = \frac{4}{3}\left(\frac{2}{\mu_T} + \frac{1}{\mu_L}\right)f_-^3$
	$F_{[001]}^B = 0$
	$F_{[1\bar{1}0]}^B = \frac{4}{3}\left[\left(\frac{2}{\mu_T} + \frac{1}{\mu_L}\right) - 2\left(\frac{1}{\mu_T} - \frac{1}{\mu_L}\right)\mathcal{E}_x\mathcal{E}_y\right]f_-^3$
	$F_{[110]}^B = \frac{4}{3}\left[\left(\frac{2}{\mu_T} + \frac{1}{\mu_L}\right) + 2\left(\frac{1}{\mu_T} - \frac{1}{\mu_L}\right)\mathcal{E}_x\mathcal{E}_y\right]f_-^3$
	[111] stress
$\Delta E^a = \frac{D_1^1}{\sqrt{3}}(s_{11} + 2s_{12})T + \frac{D_1^5}{2\sqrt{3}}s_{44}T$	$F_{[1\bar{1}0]}^a = F_{[11\bar{2}]}^a = \frac{2}{3}\left[\left(\frac{2}{\mu_T} + \frac{1}{\mu_L}\right) - 2\left(\frac{1}{\mu_T} - \frac{1}{\mu_L}\right)(\mathcal{E}_x\mathcal{E}_y + \mathcal{E}_y\mathcal{E}_z + \mathcal{E}_z\mathcal{E}_x)\right]f^0$
	$F_{[111]}^a = 0$
$\Delta E^b = \frac{D_1^1}{\sqrt{3}}(s_{11} + 2s_{12})T - \frac{D_1^5}{6\sqrt{3}}s_{44}T + \frac{\sqrt{2}}{3\sqrt{3}}\mathfrak{D}_3^5s_{44}T$	$F_{[1\bar{1}0]}^b = \frac{1}{9}\left[\left(\frac{2}{\mu_T} + \frac{1}{\mu_L}\right) + 2\left(\frac{1}{\mu_T} - \frac{1}{\mu_L}\right)\mathcal{E}_x\mathcal{E}_y\right]f_+^5$
	$F_{[11\bar{2}]}^b = \frac{1}{27}\left[3\left(\frac{2}{\mu_T} + \frac{1}{\mu_L}\right) - 2\left(\frac{1}{\mu_T} - \frac{1}{\mu_L}\right)(\mathcal{E}_x\mathcal{E}_y - 2\mathcal{E}_y\mathcal{E}_z - 2\mathcal{E}_z\mathcal{E}_x)\right]f_+^5$
	$F_{[111]}^b = \frac{16}{27}\left[3\left(\frac{2}{\mu_T} + \frac{1}{\mu_L}\right) + 2\left(\frac{1}{\mu_T} - \frac{1}{\mu_L}\right)(\mathcal{E}_x\mathcal{E}_y + \mathcal{E}_y\mathcal{E}_z + \mathcal{E}_z\mathcal{E}_x)\right]f_+^5$
$\Delta E^c = \frac{D_1^1}{\sqrt{3}}(s_{11} + 2s_{12})T - \frac{D_1^5}{6\sqrt{3}}s_{44}T - \frac{\sqrt{2}}{3\sqrt{3}}\mathfrak{D}_3^5s_{44}T$	$F_{[1\bar{1}0]}^c = \frac{1}{3}\left[3\left(\frac{2}{\mu_T} + \frac{1}{\mu_L}\right) - 2\left(\frac{1}{\mu_T} - \frac{1}{\mu_L}\right)(\mathcal{E}_x\mathcal{E}_y - 2\mathcal{E}_y\mathcal{E}_z - 2\mathcal{E}_z\mathcal{E}_x)\right]f_-^5$
	$F_{[11\bar{2}]}^c = \left[\left(\frac{2}{\mu_T} + \frac{1}{\mu_L}\right) + 2\left(\frac{1}{\mu_T} - \frac{1}{\mu_L}\right)\mathcal{E}_x\mathcal{E}_y\right]f_-^5$
	$F_{[111]}^c = 0$
	$f_+^3 = f^0 + \frac{1}{\sqrt{3}}(s_{11} - s_{12})Tf^3$
	$f_-^3 = f^0 - \frac{1}{\sqrt{3}}(s_{11} - s_{12})Tf^3$
	$f_+^5 = f^0 + \frac{1}{3\sqrt{3}}s_{44}Tf^5$
	$f_-^5 = f^0 - \frac{1}{3\sqrt{3}}s_{44}Tf^5$
	$f^s = 2\langle 0   p_{3\alpha}   \psi_{3\alpha} \rangle \langle \psi_{3\alpha}^s   p_{3\alpha}   0 \rangle$ ; $s=3$ for [001] stress, $s=5$ for [111] stress, $\alpha = (x-y)/\sqrt{2}$ and $(x+y-2z)/\sqrt{6}$

<sup>a</sup> These energy shifts have been calculated by E. O. Kane. See Table VII of Ref. 9.

#### IV. RESULTS

##### A. In the absence of strain

Figure 1 shows a Schottky-barrier ER spectrum of Si in the energy range from 3.2 to 3.6 eV at room temperature. The spectrum shown in Fig. 1

is rather complicated but it is reasonable to consider that two different structures are found in this spectrum. One is a dominant structure ( $S_I$ ) and the other is a weak one ( $S_{II}$ ) which is superimposed on the low-energy negative peak of the  $S_I$  structure. We have determined the band-edge

TABLE III. Energy shift  $\Delta E$  and electroreflectance form factor  $F$  for the degenerate  $U_5$  band in the  $\Delta$  direction. Spin-orbit interaction is neglected. The factor  $F$  has been summed over the six equivalent components. The subscript of  $F$  denotes the polarization of the light.

Energy shift <sup>a</sup>	Electroreflectance form factor
[001] stress	
$\Delta E^A = \frac{D_1^1}{\sqrt{3}}(s_{11} + 2s_{12})T + \sqrt{\frac{2}{3}}D_1^3(s_{11} - s_{12})T$	$F_{[100]}^A = F_{[010]}^A = F_{[\bar{1}\bar{1}0]}^A = F_{[110]}^A = 2\left[\frac{1}{\mu_T} - \left(\frac{1}{\mu_T} - \frac{1}{\mu_L}\right)\mathcal{G}_z^2\right]f^0$
	$F_{[001]}^A = 0$
$\Delta E^B = \frac{D_1^1}{\sqrt{3}}(s_{11} + 2s_{12})T - \frac{D_1^3}{\sqrt{6}}(s_{11} - s_{12})T + \frac{\mathcal{D}_3}{\sqrt{2}}(s_{11} - s_{12})T$	$F_{[100]}^B = F_{[010]}^B = F_{[\bar{1}\bar{1}0]}^B = F_{[110]}^B = 0$
	$F_{[001]}^B = 2\left[\left(\frac{1}{\mu_T} + \frac{1}{\mu_L}\right) + \left(\frac{1}{\mu_T} - \frac{1}{\mu_L}\right)\mathcal{G}_z^2\right]f_+^3$
$\Delta E^C = \frac{D_1^1}{\sqrt{3}}(s_{11} + 2s_{12})T - \frac{D_1^3}{\sqrt{6}}(s_{11} - s_{12})T - \frac{\mathcal{D}_3}{\sqrt{2}}(s_{11} - s_{12})T$	$F_{[100]}^C = 2\left[\frac{1}{\mu_T} - \left(\frac{1}{\mu_T} - \frac{1}{\mu_L}\right)\mathcal{G}_y^2\right]f_-^3$
	$F_{[010]}^C = 2\left[\frac{1}{\mu_T} - \left(\frac{1}{\mu_T} - \frac{1}{\mu_L}\right)\mathcal{G}_x^2\right]f_-^3$
	$F_{[001]}^C = 0$
	$F_{[\bar{1}\bar{1}0]}^C = F_{[110]}^C = \left[\left(\frac{1}{\mu_T} + \frac{1}{\mu_L}\right) + \left(\frac{1}{\mu_T} - \frac{1}{\mu_L}\right)\mathcal{G}_z^2\right]f_-^3$
[111] stress	
$\Delta E^a = \frac{D_1^1}{\sqrt{3}}(s_{11} + 2s_{12})T + \frac{\mathcal{D}_4}{6}s_{44}T$	$F_{[\bar{1}\bar{1}0]}^a = \frac{1}{2}\left[\left(\frac{1}{\mu_T} + \frac{1}{\mu_L}\right) + \left(\frac{1}{\mu_T} - \frac{1}{\mu_L}\right)\mathcal{G}_z^2\right]f_+^4$
	$F_{[11\bar{2}]}^a = \frac{1}{6}\left[\left(\frac{5}{\mu_T} + \frac{1}{\mu_L}\right) - 3\left(\frac{1}{\mu_T} - \frac{1}{\mu_L}\right)\mathcal{G}_z^2\right]f_+^4$
	$F_{[111]}^a = \frac{4}{3}\left(\frac{2}{\mu_T} + \frac{1}{\mu_L}\right)f_+^4$
$\Delta E^b = \frac{D_1^1}{\sqrt{3}}(s_{11} + 2s_{12})T - \frac{\mathcal{D}_4}{6}s_{44}T$	$F_{[\bar{1}\bar{1}0]}^b = \frac{1}{2}\left[\left(\frac{5}{\mu_T} + \frac{1}{\mu_L}\right) - 3\left(\frac{1}{\mu_T} - \frac{1}{\mu_L}\right)\mathcal{G}_z^2\right]f_-^4$
	$F_{[11\bar{2}]}^b = \frac{3}{2}\left[\left(\frac{1}{\mu_T} + \frac{1}{\mu_L}\right) + \left(\frac{1}{\mu_T} - \frac{1}{\mu_L}\right)\mathcal{G}_z^2\right]f_-^4$
	$F_{[111]}^b = 0$
	$f_+^3 = f^0 + \frac{1}{\sqrt{2}}(s_{11} - s_{12})Tf^3$ $f_-^3 = f^0 - \frac{1}{\sqrt{2}}(s_{11} - s_{12})Tf^3$
	$f_+^4 = f^0 + \frac{1}{6}s_{44}Tf^4$ $f_-^4 = f^0 - \frac{1}{6}s_{44}Tf^4$
	$f^s \equiv 2 \langle 0   p_{5\alpha}^\dagger   \psi_{5\alpha} \rangle \langle \psi_{5\alpha}^s   p_{5\alpha}   0 \rangle$ ; $s=3$ for [001] stress, $s=4$ for [111] stress, $\alpha=x$ and $y$

<sup>a</sup> These energy shifts have been calculated by E. O. Kane. See Table III of Ref. 9.

parameters by performing a least-squares fit of the three- and two-dimensional low-field resonant functions to the spectra. The determined parameters are listed in Table IV with values quoted from other modulation measurements in the literature. The calculated line shapes are also illustrated in Fig. 1. In the best-fit procedures, the field inhomogeneity effect was neglected in

our samples and the coefficient of the contact exciton effect was considered as an adjustable parameter. The Seraphin coefficients of the air-Ni-Si three-phase system were used.<sup>49</sup> The values of the Seraphin coefficients calculated from the reflectivity of Si and Ni are plotted in Fig. 2 as a parameter of the thickness of the Ni film. As shown in Fig. 2,  $\alpha$  and  $\beta$  both decrease

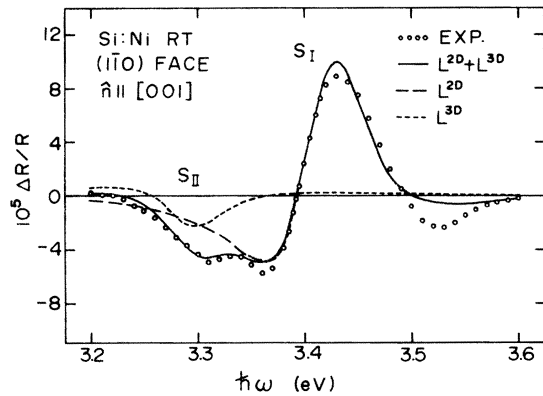


FIG. 1. Schottky-barrier electroreflectance spectrum of Si at room temperature (RT). Open circles are the experimental results taken on (110) face for [001] polarization in the low-field modulation limit. Short-dashed and long-dashed lines are the calculated three-dimensional ( $L^{3D}$ ) and two-dimensional ( $L^{2D}$ ) line shapes, respectively. Solid line is the sum of the two.

and become rather structureless upon increasing the thickness of the Ni film. When we use the estimated thickness of the Ni film (10 nm) in our samples,  $\alpha \cong \beta > 0$  at 3.3 eV and  $|\alpha| < |\beta|$ ,  $\beta > 0$  around 3.4 eV. Therefore, the  $S_{II}$  structure of  $\Delta R/R$  is affected by  $\Delta\epsilon_1$  and  $\Delta\epsilon_2$  in almost the same amount and the  $S_I$  structure is nearly  $\Delta\epsilon_2$  dominant. We discuss the results obtained from the line shape analysis. As shown in Fig. 1 the  $S_I$  structure was fitted by the two-dimensional resonant function only because of the fact that it gives better-fitted results than the three-dimensional function. Almost the same values of the critical-point energy are obtained for both line-shape functions. Note, however, that it is necessary to determine the type of a critical point and the broadening energy with the three-dimensional function. Then, the critical points related to the  $S_I$  and  $S_{II}$  structures are determined to be three-dimensional  $M_1$  and  $M_0$  types, respectively.

Next we consider the symmetry assignment for the critical points related to the  $S_I$  and  $S_{II}$  structures. The polarization anisotropies of the Schottky-barrier ER spectra of Si are shown in Fig. 3. Data were taken on (110) face at 77 K. The top pair of curves was obtained at a low-field condition with two principal orthogonal polarizations,  $\hat{n} \parallel [001]$  (dashed line) and  $\hat{n} \parallel [110]$  (solid line). The bottom pair of curves was obtained at a low-field condition with two principal orthogonal polarizations,  $\hat{n} \parallel [111]$  (dashed line) and  $\hat{n} \parallel [11\bar{2}]$  (solid line). The line shapes of these spectra are analogous to that obtained by Forman *et al.*<sup>15</sup> in the transverse ER measurements. As seen in Fig. 3, the  $S_I$  and  $S_{II}$  structures, especially the latter one,

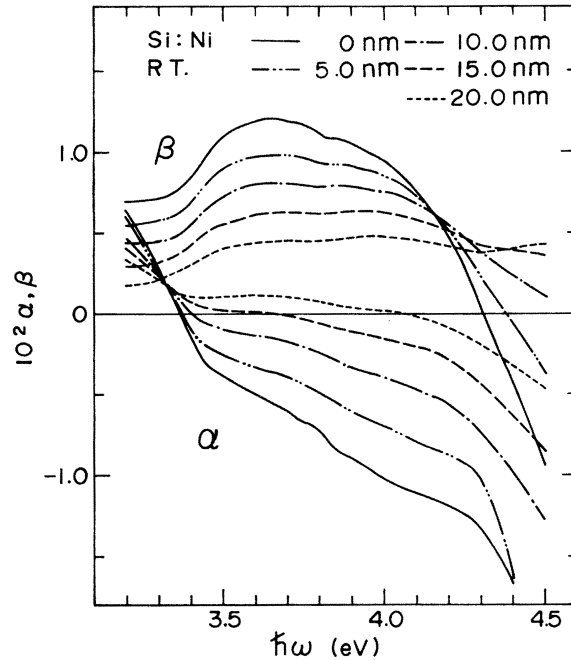


FIG. 2. Seraphin coefficients of air-Ni-Si three-phase system calculated from the reflectivity spectra of Ni and Si. The results are shown with the thickness of Ni film as a parameter.

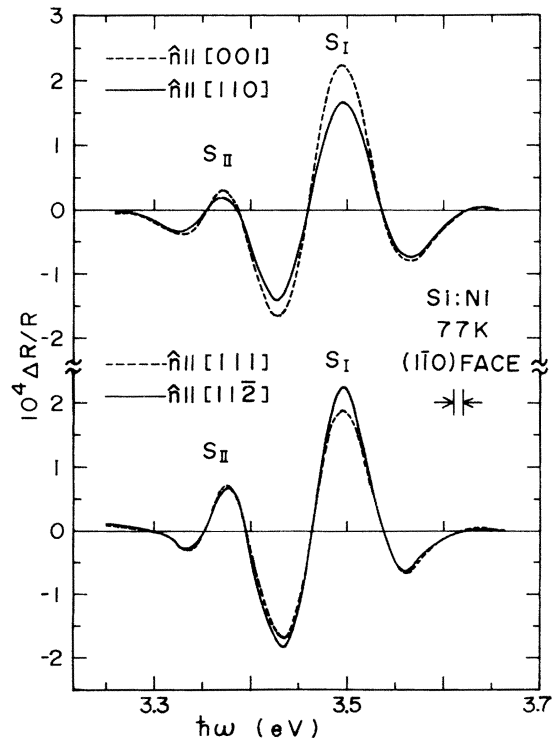


FIG. 3. Polarization anisotropies of the Schottky-barrier electroreflectance of Si. Data are taken on (110) face at 77 K in the low-field modulation limit.

TABLE IV. Critical-point parameters of Si determined from electroreflectance (ER), wavelength-modulated reflectance (WMR), and thermorelectance (TR) measurements. RT stands for room temperature.

	This work ER (RT)	Grover and Handler <sup>a</sup> ER (RT)	Lukeš <i>et al.</i> <sup>b</sup> ER (90 K)	Serapin and Bottka <sup>c</sup> ER (95 K)
$E_g$ (eV)	$3.412 \pm 0.005$	$3.360 \pm 0.016$	$3.44 \pm 0.05$	3.41
$\Gamma$ (eV)	$0.060 \pm 0.005$	$0.05322 \pm 0.00236$		0.035
Symmetry	$\Lambda_3^y(L_3^y) \rightarrow \Lambda_1^y(L_1^y)$	$\Lambda_3^y \rightarrow \Lambda_1^y$		
Type (reduced-mass relations)	$M_1^{3D}$ $(\mu_T \ll  \mu_L , \mu_T > 0, \mu_L < 0)$	$M_0^{2D}$	$M_1^{3D}$	$M_1^{3D}$
$E_g$ (eV)	$3.294 \pm 0.005$	$3.281 \pm 0.007$	$3.34 \pm 0.05$	3.33
$\Gamma$ (eV)	$0.060 \pm 0.005$	$0.05177 \pm 0.01286$		0.035
Symmetry	$\Delta_5^y \rightarrow \Delta_1^y$ near $\Gamma$		$\Gamma_{25'}^y \rightarrow \Gamma_{15}^y$	
Type	$M_0^{3D}$	$M_1^{3D}$	$M_0^{3D}$	$M_0^{3D}$
	Forman <i>et al.</i> <sup>d</sup> ER	Zucca <i>et al.</i> <sup>e</sup> WMR (5 K)	Braunstein and Welkowsky <sup>f</sup> WMR (80 K)	Matatagui <i>et al.</i> <sup>g</sup> TR (77 K)
$E_g$ (eV)	$3.485 \pm 0.015$	$3.45 \pm 0.004$	3.41	3.43
$\Gamma$ (eV)				
Symmetry	$\Lambda_3^y \rightarrow \Lambda_1^y$	$\Lambda_3^y \rightarrow \Lambda_1^y$	$\Delta_5^y \rightarrow \Delta_1^y$	
Type (reduced-mass relations)		$M_1^{3D}$	$M_1^{3D}$	$M_1^{3D}$
$E_g$ (eV)	$3.370 \pm 0.030$	$3.40 \pm 0.008$	3.36	3.32
$\Gamma$ (eV)				
Symmetry	$\Gamma_{25'}^y \rightarrow \Gamma_{15}^y$	$\Delta_5^y \rightarrow \Delta_1^y$	$\Gamma_{25'}^y \rightarrow \Gamma_{15}^y$	
Type			$M_0^{3D}$	$M_0^{3D}$

<sup>a</sup> Reference 14.<sup>b</sup> Reference 46.<sup>c</sup> Reference 11.<sup>d</sup> Reference 15; see also Ref. 47.<sup>e</sup> Reference 16; see also Ref. 36.<sup>f</sup> Reference 27.<sup>g</sup> Reference 48.

become sharper at 77 K than at room temperature. The lower-energy side of the  $S_I$  and the higher-energy side of the  $S_{II}$  structures interfere with each other considerably at 77 K. Therefore, the exact best-fit analysis is difficult. We discuss the  $S_I$  structure first. From the results shown in Fig. 3, we obtain polarization anisotropies  $|r| = (\Delta R/R)_{[001]} / (\Delta R/R)_{[110]} = 1.35 \pm 0.05$  and  $|s| = (\Delta R/R)_{[111]} / (\Delta R/R)_{[1\bar{1}2]} = 0.86 \pm 0.05$  at the positive peak of the structure. The experimental results can be compared to the theoretical criteria for high-symmetry critical points listed in Table I. First, the  $\Gamma$  critical point may be ruled out, since it gives the isotropic polarization effect. Second, the  $\Delta$  critical point may be ruled out, since the com-

binations of the observed polarization anisotropies and the critical point type ( $M_1$ ) conflict with the conditions of the  $\Delta$  critical point with  $U_1$  and  $U_5$  symmetry. Third, the  $\Lambda$  (or  $L$ ) critical point with  $U_1$  (or  $U_{2-}$ ) symmetry may be ruled out because of the same reasons as in the case of the  $\Delta$  critical point. For the  $\Lambda$  (or  $L$ ) critical point with  $U_3$  (or  $U_{3-}$ ) symmetry, the calculated polarization anisotropies become  $r = \frac{4}{3}$  and  $s = \frac{10}{11}$  if we assume the reduced-mass relations to be  $|\mu_T| \ll |\mu_L|$ ,  $\mu_T > 0$ , and  $\mu_L < 0$ . In this case, the experimental results are well explained. Finally, the  $\Sigma$  critical point may be ruled out, since it cannot explain the stress effects, as will be shown in Sec. IV B. Thus, we conclude that the  $S_I$  structure is attributed to the

$\Lambda$  (or  $L$ ) critical point with  $U_3$  (or  $U_{3-}$ ) symmetry [ $\Lambda_3^v \rightarrow \Lambda_1^c$  (or  $L_3^v \rightarrow L_1^c$ ) in Si]. In addition, we conclude from the mass relation,  $\mu_T \ll |\mu_L|$ , that the critical point is rather two-dimensional  $M_0$  type ( $\mu_T > 0$ ). We consider the  $S_{II}$  structure next. In Fig. 3, the polarization anisotropies are found to be  $|\gamma| = 1.4 \pm 0.1$  and  $|s| = 1.0 \pm 0.1$  at the positive peak of the structure. The results can also be compared to the theoretical criteria listed in Table I. In this case, however, we cannot determine the location  $\vec{K}_0$  of the critical point uniquely from the above method of symmetry analysis. The transitions  $\Gamma_{25}^v \rightarrow \Gamma_{15}^c$  and  $\Delta_5^v \rightarrow \Delta_1^c$  near the  $\Gamma$  point may be possible from the results of band-structure calculations.<sup>56</sup> The symmetry location of the  $S_{II}$  structure will be discussed further in Sec. IV B.

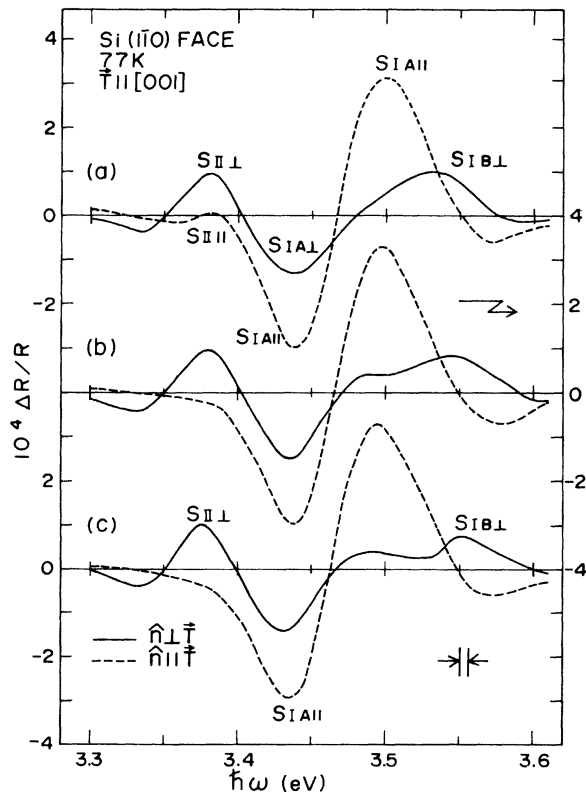


FIG. 4. Schottky-barrier electroreflectance spectra of Si under uniaxial stress (compression) along the [001] direction: (a)  $T = -3.84 \times 10^9$  dyn/cm<sup>2</sup>; (b)  $T = -5.35 \times 10^9$  dyn/cm<sup>2</sup>; (c)  $T = -6.97 \times 10^9$  dyn/cm<sup>2</sup>. Data are taken on (110) face at 77 K in the low-field modulation limit. Solid lines are the spectra for  $\hat{n} \perp \hat{T}$  and the dashed lines for  $\hat{n} \parallel \hat{T}$ .  $S_{I A \perp}$  (or  $S_{I A \parallel}$ ),  $S_{II \perp}$  (or  $S_{II \parallel}$ ), etc., are the split-off structures of  $S_I$  and  $S_{II}$  under [001] stress with perpendicular (or parallel) polarization.

#### B. In the presence of strain

Schottky-barrier ER spectra of Si for compression stresses along the [001] and [111] directions are shown in Figs. 4 and 5, respectively, with light polarized parallel and perpendicular to the stress axis. The stress-induced energy shifts and amplitude changes are apparent in both cases. The spectra without stress are shown in Fig. 3, where the top and bottom pair of curves correspond to the [001] and [111] stress configurations, respectively.

First we discuss the  $S_I$  structure. The dependences of the peak energies of the structure for the [001] and [111] stresses are shown in Figs. 6(a) and 6(b), respectively, where the energy positions of positive and negative peaks are plotted together. In the case of [001] stress, the  $S_I$  structure splits into two parts for transverse polarization, i.e., one shifts to higher energy and the other to lower energy; and for parallel polarization the structure

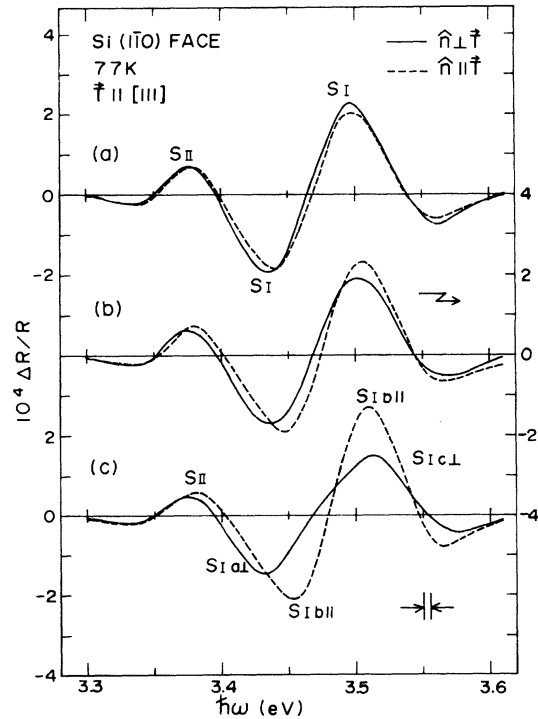


FIG. 5. Schottky-barrier electroreflectance spectra of Si under uniaxial stress (compression) along the [111] direction: (a)  $T = -1.87 \times 10^9$  dyn/cm<sup>2</sup>; (b)  $T = -5.65 \times 10^9$  dyn/cm<sup>2</sup>; (c)  $T = -8.78 \times 10^9$  dyn/cm<sup>2</sup>. Data are taken on (110) face at 77 K in a low-field modulation limit. Solid lines are the spectra for  $\hat{n} \perp \hat{T}$  and dashed lines for  $\hat{n} \parallel \hat{T}$ .  $S_{I a \perp}$ ,  $S_{I b \parallel}$ , etc., are the split-off structures of  $S_I$  under [111] stress with perpendicular and parallel polarizations.

shifts to lower energy without any splitting. In the case of [111] stress, the polarization-dependent splittings and shifts of the structure are also observed, though the shifts are smaller: For perpendicular polarization the structure splits into two parts, i.e., one shifts to higher energy and the other to lower energy; for parallel polarization the structure shifts to higher energy without any splitting. These energy shifts and splittings of the  $S_1$  structure are well explained by the stress effects of the degenerate  $\Lambda_3^c-\Lambda_1^c$  (or  $L_3^-L_1^c$ ) critical point in the following way. In the case of [001] stress, we find from Table II that the  $U_3$  (or  $U_{3-}$ ) pair band splits into two parts due to intraband splitting; one component labeled  $A$  is allowed for both  $\hat{n} \parallel \vec{T}$  and  $\hat{n} \perp \vec{T}$ , while the other component  $B$  is allowed only for  $\hat{n} \perp \vec{T}$ . Moreover, the intensity ratios of the split bands for parallel and perpendicular polarization with zero stress are  $F_{\parallel}^A:F_{\parallel}^B=8:0$  and  $F_{\perp}^A:F_{\perp}^B=3:3$  in our experimental configuration; the unit vector of the applied electric field  $\hat{\epsilon}=(1/\sqrt{2}, -1/\sqrt{2}, 0)$  and the effective mass relation is  $\mu_{\tau} \ll |\mu_L|$ . In the case of [111] stress, we

find from Table II that the  $U_3$  (or  $U_{3-}$ ) pair band splits into three parts due to interband and intraband splittings: Two components labeled  $a$  and  $c$  are allowed only for  $\hat{n} \perp \vec{T}$  and the other component  $b$  is allowed for both  $\hat{n} \parallel \vec{T}$  and  $\hat{n} \perp \vec{T}$ . The intensity ratios of the split bands for parallel and perpendicular polarization with zero stress are  $F_{\parallel}^a:F_{\parallel}^b:F_{\parallel}^c=0:80:0$  and  $F_{\perp}^a:F_{\perp}^b:F_{\perp}^c=54:7:27$ . Then, for  $\hat{n} \perp \vec{T}$  the structure due to the intermediate component  $b$  is negligibly small and the two components  $a$  and  $c$  will be observed. We have calculated the deformation-potential parameters from the stress-induced energy shifts using the compliance constants at 77 K (in units of  $10^{-12}$  cm<sup>2</sup>/dyn)<sup>57</sup>;  $s_{11}=0.762$ ,  $s_{12}=-0.213$ , and  $s_{44}=1.249$ . The results are listed in Table V. The stress-induced amplitude changes of  $\Delta R/R$  are also explained by the stress effects of the degenerate  $\Lambda_3^c-\Lambda_1^c$  (or  $L_3^-L_1^c$ ) critical point. Plotted in Figs. 7(a) and 7(b) are the amplitude changes of  $\Delta R/R$  as a function of [001] and [111] stresses, respectively. In general, the

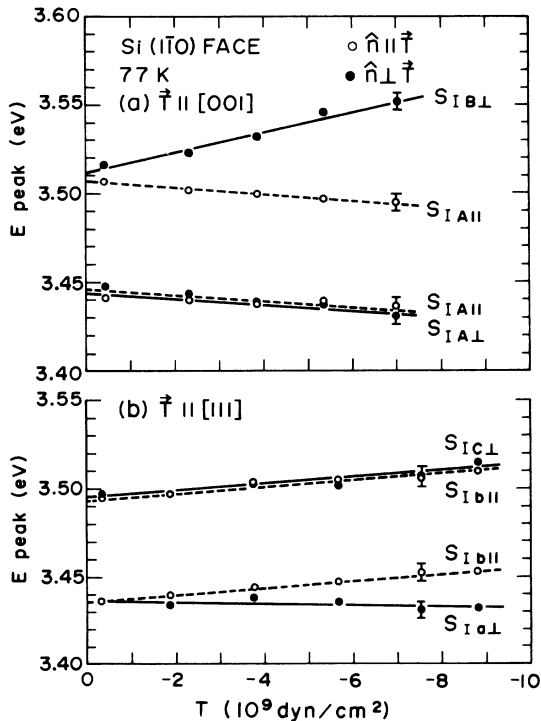


FIG. 6. Stress dependences of the peak energies of the  $S_1$  structure. The energy positions of positive and negative peaks are plotted together. (a)  $\vec{T} \parallel [001]$  and (b)  $\vec{T} \parallel [111]$ . Solid lines are obtained for  $\hat{n} \perp \vec{T}$  and dashed lines for  $\hat{n} \parallel \vec{T}$ .

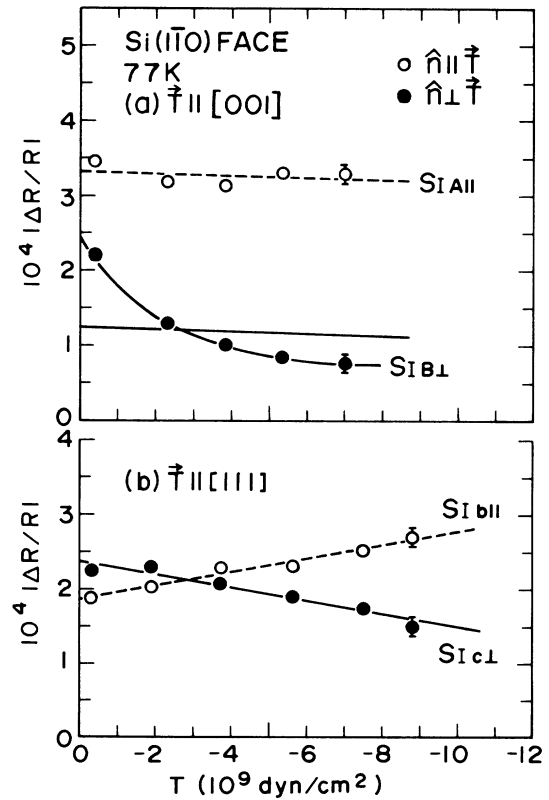


FIG. 7. Amplitude changes of the positive peak of the  $S_1$  structure as a function of uniaxial stresses along (a) the [001] direction and (b) the [111] direction. Solid lines are obtained for  $\hat{n} \perp \vec{T}$  and dashed lines for  $\hat{n} \parallel \vec{T}$ .

TABLE V. Deformation potentials of the  $A_3^3(L_3^3) - A_1^1(L_1^1)$  critical point of Si. The previously reported values of Si and Ge and some pressure coefficients of Si are also listed for comparison. RT stands for room temperature.

	This work <sup>a</sup> Si (77 K)	Pollak and Rubloff <sup>b</sup> Si (77 K)	Sell and Kane <sup>c</sup> Ge (RT)	Pressure coefficients	
				Experiment Si	Calculated Si
$D_1^1$ (eV)	$-9.8 \pm 1.3$	$-8 \pm 1$	$-9.7 \pm 1$		
$D_1^5$ (eV)	$6.5 \pm 1.4$	$10 \pm 2$	$7.5 \pm 0.8$		
$D_3^3(D_3^3)$ (eV)	$4.7 \pm 0.5$	$5 \pm 1$	$2.2^{+1}_{-0.5}$		
$D_3^5(D_3^5)$ (eV)	$3.0 \pm 1.7$	$4 \pm 1$	$1.5^{+0.6}_{-0.3}$		
$\frac{dE_g}{dP}$	$5.7 \pm 0.8$			$5.2 \pm 0.5$ <sup>d</sup>	$5.3$ (RT) <sup>f</sup>
				$6.2 \pm 0.4$ <sup>e</sup>	$4.4$ <sup>g</sup>
					$5.7$ <sup>h</sup>
					$5.6 \pm 0.6$ (RT) <sup>i</sup>
					$4.8$ <sup>j</sup>
					$5.9$ <sup>k</sup>

( $10^{-6}$  eV/bar)

<sup>a</sup> See Ref. 58.

<sup>b</sup> Reference 10.

<sup>c</sup> Reference 59.

<sup>d</sup> Reference 60.

<sup>e</sup> Reference 17.

<sup>f</sup> Reference 20. The conversion from their units to ours is based on the identity  $-1.00$  eV/(unit dilatation) =  $1.02 \times 10^{-6}$  eV/bar for Si at room temperature.

<sup>g</sup> Reference 19. The conversion from their units to ours is based on the identity  $1.00$  eV/atm =  $0.987$  eV/bar.

<sup>h</sup> Reference 61.

<sup>i</sup> Reference 62. See Ref. f for the conversion from their units to ours.

<sup>j</sup> Reference 22.

<sup>k</sup> Reference 63. The conversion from their units to ours is based on the identity  $1.00$  eV cm<sup>2</sup>/kg =  $1.02$  eV/bar.

observed amplitude changes consist of substantial stress-induced change and unsubstantial change due to the splitting of the structure. We find in Fig. 7(a) a large and nonlinear change in the amplitude of  $\Delta R/R$  for [001] stress and perpendicular polarization. It seems to be due mainly to the separation of the structure, because the energy shifts  $\Delta E^A$  and  $\Delta E^B$  are relatively large in this configuration [as shown in Fig. 6(a)]. The theoretical expressions of the ER form factor  $F$  for [001] stress are presented in Table II and, therefore, the substantial changes of  $\Delta R/R$  in this case may be shown with solid lines in Fig. 7(a); the optical-matrix-element ratio was estimated to be  $f^3/10^3f^0 \cong 0$ . This ratio shows the admixture of wave functions from the symmetry multiplet<sup>9</sup> under [001] stress, and in this case the bands are well separated and the admixture of wave functions between the split bands is very small. On the other hand, the amplitude changes of  $\Delta R/R$  for [111] stress shown in Fig. 7(b) seem to represent the substantial changes of the optical matrix element, because the energy shifts of the structure shown in Fig. 6(b) are relatively small. The observed amplitude changes are also explained by the equations given

in Table II, and we can estimate the optical-matrix-element ratio,  $f^5/10^3f^0 = -0.20 \pm 0.02$ . In this case, the admixture of wave functions between the split bands is relatively large.

The observed uniaxial-stress effects of the  $S_{II}$  structure described above cannot be explained by the behaviors of any  $\Sigma$  critical point under stress. Since all the irreducible pair bands  $U_1$ ,  $U_2$ , and  $U_3$  in the  $\Sigma$  direction are nondegenerate, the ER form factor  $F$  is not changed with stress,<sup>64</sup> ignoring the mixing between pair bands with different symmetries. This is apparently incompatible with the observed amplitude changes of  $\Delta R/R$  with stress.

Next, we consider the  $S_{II}$  structure. Figures 8(a) and 8(b) show the dependences of positive peak energy for [001] and [111] stresses, respectively. As seen in Fig. 8, the structure splits into two parts for both stress directions: The structure shifts to higher energy for parallel polarization and to lower energy for perpendicular polarization, though these shifts are very small. We also show the amplitude changes as a function of stress in Fig. 9. It is interesting that the amplitude of  $\Delta R/R$  for parallel polarization decreases as the stress increases in the [001] direction and the

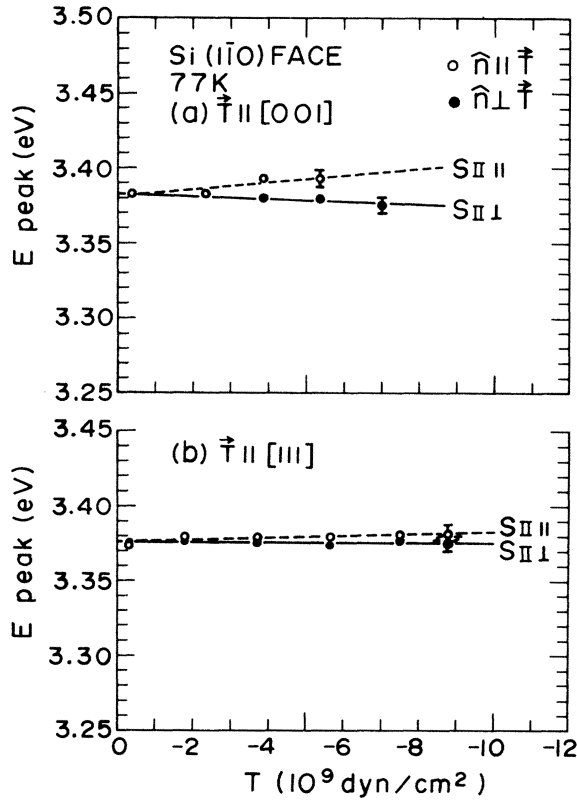


FIG. 8. Stress dependences of the peak energies of the  $S_{II}$  structure. (a)  $\vec{T} \parallel [001]$  and (b)  $\vec{T} \parallel [111]$ . Solid lines are obtained for  $\hat{n} \perp \vec{T}$  and dashed lines for  $\hat{n} \parallel \vec{T}$ .

structure disappears at about  $7 \times 10^9 \text{ dyn/cm}^2$ , while the amplitude for perpendicular polarization does not change with stress. From these results, we can obtain information about the location  $\vec{K}_0$  of the critical point related to the  $S_{II}$  structure if we assume the high-symmetry critical point. First, the  $\Delta$  critical point with  $U_1$  symmetry, the  $\Lambda$  (or  $L$ ) critical point with  $U_1$  (or  $U_{2-}$ ) symmetry, and the  $\Sigma$  critical point with  $U_1$ ,  $U_2$ , and  $U_3$  symmetry may be ruled out, since these critical points are strain-decoupled and, therefore, the optical matrix elements will not be changed by strain.<sup>9</sup> Second, the  $\Lambda$  (or  $L$ ) critical point with  $U_3$  (or  $U_{3-}$ ) symmetry may be ruled out, since the observed energy shifts and amplitude changes of the  $S_{II}$  structure are much different from those of the  $S_I$  structure, which is attributed to the critical point of this symmetry. Third, the  $\Gamma$  critical point with  $U_{4-}$  symmetry ( $\Gamma_{25'}^v \rightarrow \Gamma_{15}^c$  in Si) may be ruled out, since the theoretical equations for the  $\Gamma$  transition cannot explain the amplitude changes for [001] stress. From Eq. (3.49) in Ref. 9, the ER form factor  $F$  for [001] stress and parallel polarization may be written

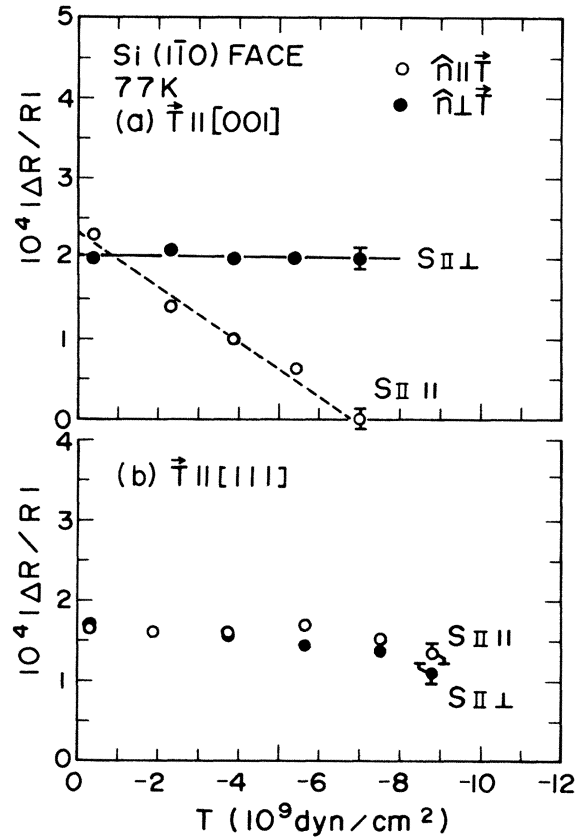


FIG. 9. Amplitude changes of the positive peak of the  $S_{II}$  structure as a function of uniaxial stresses along (a) the [001] direction and (b) the [111] direction. Solid lines are obtained for  $\hat{n} \perp \vec{T}$  and dashed lines for  $\hat{n} \parallel \vec{T}$ .

$$F_{\parallel} = F_{[001]} = \frac{1}{\mu} \left( f^0 + \frac{2\sqrt{2}}{\sqrt{3}} (s_{11} - s_{12}) T f^3 \right), \quad (4.1)$$

and for perpendicular polarization,

$$F_{\perp} = F_{[110]} = \frac{1}{\mu} \left( f^0 - \frac{\sqrt{2}}{\sqrt{3}} (s_{11} - s_{12}) T f^3 \right). \quad (4.2)$$

Thus,  $(\Delta R/R)_{\perp}$  for [001] stress should increase by  $\frac{1}{2}$  times less than  $(\Delta R/R)_{\parallel}$  if  $(\Delta R/R)_{\parallel}$  decreases. The remaining high-symmetry critical points along the  $\Delta$  axis with  $U_5$  symmetry ( $\Delta_5^v \rightarrow \Delta_1^c$  near  $\Gamma$  in Si) are now more likely to explain the experimental results due to the manifold splittings for [001] stress as shown in Table III. The more detailed analysis, however, is difficult, since the observed energy shifts and amplitude changes under stress are quite small. We may conclude at the present stage that the  $S_{II}$  structure is due to the  $\Delta$  critical point with  $U_5$  symmetry if we assume high-symmetry critical points. This assignment does not conflict with the results of the symmetry analysis

in the absence of strain. The effective mass relations are  $\mu_T/\mu_L = 1-3$ ,  $\mu_T > 0$ , and  $\mu_L > 0$  in this case.

## V. DISCUSSION

The experimental results of this paper obtained from the line-shape analysis in the absence of strain are summarized in Table IV, together with the data previously obtained with other modulation techniques. The critical-point energy and the phenomenological broadening energy can now be obtained very accurately from ER line shapes; these values are estimated by Aspnes's three-point method<sup>5</sup> and more precisely by a method of least-squares fit. When two or more structures interfere with each other, however, which is usually seen in the higher-energy region, the best-fit analysis becomes more complicated. Our results of the 3.4-eV structures of Si disagree in some points with the results obtained by Grover and Handler<sup>14</sup> using the electrolyte ER technique in the flatband condition. The values of the critical-point energies determined in this work are somewhat larger than those determined by Grover and Handler. This is probably due to the difference between the line-shape functions used in the best-fit analysis (the two-dimensional electro-optic  $F$  and  $G$  functions<sup>65</sup> in their analysis and the low-field resonant functions<sup>5</sup> in this analysis), and also due to the broadening effects in such a high-energy region. Moreover, Grover and Handler have shown that the main structure was contributed to the two-dimensional  $M_0$  critical point, and the weak structure in the lower-energy side to the three-dimensional  $M_1$  critical point from the best-fit analysis on the ER line shapes. The former result is consistent with our result, i.e., the three-dimensional  $M_1$  or rather two-dimensional  $M_0$  critical point, but the latter one is not. The results of other authors listed in Table IV are in agreement with our results.

The 3.4-eV complexities of Si have been the origin of some controversy for a long time, as described in Sec. I. In this paper, the main structure in the higher-energy side is attributed conclusively to the  $\Lambda_3^v \rightarrow \Lambda_1^c$  (or  $L_3^v \rightarrow L_1^c$ ) transition from the symmetry analysis described in Sec. IV A and from the uniaxial-stress effects on the low-field ER spectra described in Sec. IV B. On the other hand, the weak structure in the lower-energy side is not determined conclusively, although at the present stage it is considered to be attributed to the  $\Delta_3^v \rightarrow \Delta_1^c$  transition near the  $\Gamma$  point. These results are in agreement with that obtained by Pollak and Rubloff<sup>10</sup> from the uniaxial-stress effects on the wavelength-modulated reflectance spectra. The above assignments are also supported by the re-

sults of the composition dependence of the Ge-Si alloy system reported by Kline *et al.*<sup>66</sup> They have found that the  $E_1$  and  $E'_0$  doublets of Ge merge into the 3.4-eV structures of Si, indicating that both the  $\Lambda$  and  $\Delta$  transitions may be responsible for this energy region.

Our measurements can also be compared to the energy-band-structure calculations of Si. In the theoretical calculations, the relative position of the energy levels rather than their precise values may be important, and the results calculated by Herman *et al.*,<sup>20</sup> Dresselhaus and Dresselhaus,<sup>21</sup> Saravia and Brust,<sup>35</sup> Van Vechten,<sup>67</sup> Zucca *et al.*,<sup>36</sup> Kane,<sup>68</sup> and Van Dyke (orthogonalized plane wave)<sup>69</sup> may be consistent with our experimental results for the structures in the energy region around 3.4-eV. It has been pointed out by Kane,<sup>33</sup> and by Saravia and Brust,<sup>35</sup> that the  $\Lambda_3$  valence and the  $\Lambda_1$  conduction bands of Si are nearly parallel from the  $\Gamma$  point to the  $L$  point in the BZ. The reduced-mass relations  $\mu_T \ll |\mu_L|$ ,  $\mu_T > 0$ , and  $\mu_L < 0$  at the  $\Lambda_3^v - \Lambda_1^c$  (or  $L_3^v - L_1^c$ ) critical point obtained from the polarization anisotropies of the low-field ER spectra verify these situations.

The deformation-potential parameters determined from the stress effects of the  $\Lambda_3^v - \Lambda_1^c$  (or  $L_3^v - L_1^c$ ) critical point are summarized in Table V together with other experimental results of Si and Ge. The values of the deformation parameters  $D_1^1$  and  $\mathfrak{D}_3^3$  determined from measurements under [001] stress are in good agreement with those determined by Pollak and Rubloff.<sup>10</sup> However, the values of  $D_1^5$  and  $\mathfrak{D}_3^3$  determined from measurements under [111] stress are smaller than those determined by them. It is probably due to the fact that the values in this work were obtained in a relatively low-stress region, while the values in their work were obtained in a high-stress region. These four values are in agreement with those determined by Sell and Kane<sup>59</sup> for the  $E_1$  structure of Ge, which may be due to the analogy of the crystal structure between Si and Ge. The pressure coefficient  $dE/dP$  is calculated from the pair band hydrostatic deformation parameter  $D_1^1$  in the form

$$\frac{dE}{dP} = -\sqrt{3} D_1^1 (s_{11} + 2s_{12}), \quad (5.1)$$

and the value determined in this work is also listed in Table V, together with previously reported experimental and calculated results for comparison. We find good agreement between our value and the other experimental and calculated values within the limit of our experimental errors.

Finally, we wish to point out the possibility that the weak  $S_{II}$  structure is contributed by the critical point located off the high-symmetry points and axes or by some critical-point set located at differ-

ent points in the BZ. With respect to this point, Saravia<sup>22</sup> has shown in his calculations that the weak structure is produced by some critical points surrounding the  $\Gamma$  point rather than the high-symmetry one and that the piezo-optical properties, especially the changes for [001] stress and parallel polarization, are explained by this critical-point set.

#### ACKNOWLEDGMENTS

The authors wish to express their gratitude to Professor C. Hamaguchi for his critical reading

of the manuscript and for helpful discussions concerning this work. They wish to express their appreciation to Dr. D. E. Aspnes of Bell Laboratories for his valuable advice about the polarization anisotropy of the low-field ER spectrum of Si. They are indebted to Dr. G. Kano of Matsushita Electronics Corp. for determining the crystal orientations of Si used in this experiment. Discussions with Professor K. Suzuki, Professor J. Nakai, and Dr. Y. Sasaki are acknowledged. This work was greatly assisted by M. Iwamoto and M. Yokogawa.

- <sup>1</sup>B. O. Seraphin and R. B. Hess, Phys. Rev. Lett. **14**, 138 (1965); B. O. Seraphin, R. B. Hess, and N. Bottka, J. Appl. Phys. **36**, 2242 (1965); B. O. Seraphin and N. Bottka, Phys. Rev. **139**, A560 (1965).
- <sup>2</sup>M. Cardona, *Modulation Spectroscopy* (Academic, New York, 1969).
- <sup>3</sup>B. O. Seraphin, R. L. Aggarwal, D. F. Blossey, P. Handler, B. Batz, I. Balsley, D. E. Aspnes, and N. Bottka, in *Semiconductors and Semimetals*, edited by R. K. Willardson and A. C. Beer (Academic, New York, 1972), Vol. 9.
- <sup>4</sup>D. E. Aspnes and J. E. Rowe, Solid State Commun. **8**, 1145 (1970); Phys. Rev. B **5**, 4022 (1972).
- <sup>5</sup>D. E. Aspnes and J. E. Rowe, Phys. Rev. Lett. **27**, 188 (1971); D. E. Aspnes, Phys. Rev. Lett. **28**, 168 (1972); **28**, 913 (1972); Surf. Sci. **37**, 418 (1973).
- <sup>6</sup>V. Rehn, Surf. Sci. **37**, 443 (1973).
- <sup>7</sup>D. E. Aspnes and A. A. Studna, Phys. Rev. B **7**, 4605 (1973).
- <sup>8</sup>F. H. Pollak and M. Cardona, Phys. Rev. **172**, 816 (1968).
- <sup>9</sup>E. O. Kane, Phys. Rev. **178**, 1368 (1969).
- <sup>10</sup>F. H. Pollak and G. W. Rubloff, Phys. Rev. Lett. **29**, 789 (1972).
- <sup>11</sup>B. O. Seraphin, Phys. Rev. **140**, A1716 (1965); B. O. Seraphin and N. Bottka, Phys. Rev. **145**, 628 (1966).
- <sup>12</sup>M. Cardona, F. H. Pollak, and K. L. Shaklee, J. Phys. Soc. Jpn. Suppl. **21**, 89 (1966); Phys. Rev. **154**, 696 (1967).
- <sup>13</sup>A. K. Ghosh, Phys. Lett. **23**, 36 (1966).
- <sup>14</sup>J. W. Grover and P. Handler, Phys. Rev. B **9**, 2600 (1974).
- <sup>15</sup>R. A. Forman, D. E. Aspnes, and M. Cardona, J. Phys. Chem. Solids **31**, 227 (1970).
- <sup>16</sup>R. R. L. Zucca and Y. R. Shen, Phys. Rev. B **1**, 2668 (1970).
- <sup>17</sup>E. Schmidt and K. Vedam, Solid State Commun. **9**, 1187 (1971).
- <sup>18</sup>D. Brust, J. C. Phillips, and F. Bassani, Phys. Rev. Lett. **9**, 94 (1962).
- <sup>19</sup>I. Goroff and L. Kleinman, Phys. Rev. **132**, 1080 (1963).
- <sup>20</sup>F. Herman, R. L. Kortum, C. D. Kuglin, and R. A. Short, in *Quantum Theory of Atoms, Molecules and the Solid State*, edited by P. O. Löwdin (Academic, New York, 1966), p. 381; J. Phys. Soc. Jpn. Suppl. **21**, 7 (1966).
- <sup>21</sup>G. Dresselhaus and M. S. Dresselhaus, Phys. Rev. **160**, 649 (1967).
- <sup>22</sup>L. R. Saravia, J. Phys. Chem. Solids **35**, 1469 (1974).
- <sup>23</sup>J. Tauc and A. Abraham, in *Proceedings of the International Conference on the Physics of Semiconductors, Prague, 1960* (Czechoslovakian Academy of Sciences, Prague, 1961), p. 375; J. Phys. Chem. Solids **20**, 190 (1961).
- <sup>24</sup>U. Gerhardt, Phys. Status Solidi **11**, 801 (1965); Phys. Rev. Lett. **15**, 401 (1965).
- <sup>25</sup>G. W. Gobeli and E. O. Kane, Phys. Rev. Lett. **15**, 142 (1965).
- <sup>26</sup>J. Koo, Y. R. Shen, and R. R. L. Zucca, Solid State Commun. **9**, 2229 (1971).
- <sup>27</sup>R. Braunstein and M. Welkowsky, in *Proceedings of the Tenth International Conference on the Physics of Semiconductors, Cambridge, Mass., 1970* (U.S. AEC Division of Technical Information, Springfield, Va., 1970), p. 439; Phys. Rev. B **5**, 497 (1972).
- <sup>28</sup>J. C. Phillips, Phys. Rev. **125**, 1931 (1962); **133**, A452 (1964); in *Solid State Physics*, edited by F. Seitz and D. Turnbull (Academic, New York, 1966), Vol. 18, p. 55.
- <sup>29</sup>D. Brust, M. L. Cohen, and J. C. Phillips, Phys. Rev. Lett. **9**, 389 (1962).
- <sup>30</sup>M. L. Cohen and J. C. Phillips, Phys. Rev. **139**, A912 (1965).
- <sup>31</sup>D. Brust, Phys. Rev. **134**, A1337 (1964); **139**, A489 (1965).
- <sup>32</sup>M. Cardona and F. H. Pollak, Phys. Rev. **142**, 530 (1966).
- <sup>33</sup>E. O. Kane, Phys. Rev. **146**, 558 (1966).
- <sup>34</sup>K. Kondo, A. Moritani, C. Hamaguchi, and J. Nakai, Solid State Commun. **15**, 1525 (1974).
- <sup>35</sup>L. R. Saravia and D. Brust, Phys. Rev. **171**, 916 (1968).
- <sup>36</sup>R. R. L. Zucca, J. P. Walter, Y. R. Shen, and M. L. Cohen, Solid State Commun. **8**, 627 (1970).
- <sup>37</sup>B. O. Seraphin, in Ref. 3, p. 1.
- <sup>38</sup>D. E. Aspnes and A. Frova, Solid State Commun. **7**, 155 (1969).
- <sup>39</sup>J. E. Rowe and D. E. Aspnes, Phys. Rev. Lett. **25**, 162 (1970).
- <sup>40</sup>Effective components of the vector potential in the star of  $\vec{k}_0 = (0, 0, k_0)$  and  $(k_0, k_0, k_0)$  are listed in Tables I and V, respectively, by E. O. Kane in Ref. 9.
- <sup>41</sup>C. Herring and E. Vogt, Phys. Rev. **101**, 944 (1956).

- <sup>42</sup>W. H. Kleiner and L. M. Roth, *Phys. Rev. Lett.* **2**, 334 (1959).
- <sup>43</sup>H. Brooks, in *Advances in Electronics and Electron Physics*, edited by L. Marton (Academic, New York, 1955), Vol. 7, p. 85.
- <sup>44</sup>G. E. Pikus and G. L. Bir, *Fiz. Tverd. Tela* **1**, 1642 (1959) [*Sov. Phys.-Solid State* **1**, 1502 (1959)].
- <sup>45</sup>Y. Sasaki, C. Hamaguchi, M. Yamada, and J. Nakai, *Rev. Sci. Instrum.* **44**, 705 (1973).
- <sup>46</sup>F. Lukes, E. Schmidt, and J. Humlíček, in *Proceedings of the Eleventh International Conference on the Physics of Semiconductors, Warsaw, Poland* (PWN-Polish Scientific Publishers, Warsaw, 1972), p. 1382.
- <sup>47</sup>R. A. Forman, W. R. Thurber, and D. E. Aspnes, *Solid State Commun.* **14**, 1007 (1974).
- <sup>48</sup>E. Matatagui, A. G. Thompson, and M. Cardona, *Phys. Rev.* **176**, 950 (1968).
- <sup>49</sup>We have calculated the three-phase Seraphin coefficients using the experimentally obtained reflectivities of Si and Ni. The data used in the calculation are as follows: Si: 0–3 eV (Philipp and Taft, Ref. 50), 3–4 eV (Moritani *et al.*, Ref. 51), 4–10 eV (Philipp and Taft, Ref. 50), 10–20 eV (Philipp and Ehrenreich, Ref. 52), above 20 eV (extrapolation equation; see Ref. 53); Ni: 0–3 eV (Ehrenreich *et al.*, Ref. 54), 3–4 eV (Moritani *et al.*, Ref. 51), 4–20 eV (Vehse and Arakawa, Ref. 55), above 20 eV (extrapolation equation; see Ref. 53).
- <sup>50</sup>H. R. Philipp and E. A. Taft, *Phys. Rev.* **120**, 37 (1960).
- <sup>51</sup>A. Moritani, K. Kondo, and J. Nakai (unpublished).
- <sup>52</sup>H. R. Philipp and H. Ehrenreich, *Phys. Rev.* **129**, 1550 (1963).
- <sup>53</sup>M. Cardona and D. L. Greenaway, *Phys. Rev.* **133**, A1685 (1964). Note that a typographical error in Eq. (5) is corrected by M. Cardona and G. Harbeke, *Phys. Rev.* **137**, A1467 (1965).
- <sup>54</sup>H. Ehrenreich, H. R. Philipp, and D. J. Olechna, *Phys. Rev.* **131**, 2469 (1963).
- <sup>55</sup>R. C. Vehse and E. T. Arakawa, *Phys. Rev.* **180**, 695 (1969).
- <sup>56</sup>See, for example, Table II and Fig. 6 of Ref. 35.
- <sup>57</sup>H. J. McSkimin, *J. Appl. Phys.* **24**, 988 (1953).
- <sup>58</sup>The values of the deformation-potential parameters listed in Table I of the previous paper (Ref. 34) are somewhat different from those listed in this table; it is due to the neglect of the intraband splitting for [111] stress in the previous paper.
- <sup>59</sup>D. D. Sell and E. O. Kane, *Phys. Rev.* **185**, 1103 (1969).
- <sup>60</sup>R. Zallen and W. Paul, *Phys. Rev.* **155**, 703 (1967).
- <sup>61</sup>C. V. de Alvarez and M. L. Cohen, *Solid State Commun.* **14**, 317 (1974).
- <sup>62</sup>D. J. Stukel and R. N. Euwema, *Phys. Rev. B* **1**, 1635 (1970).
- <sup>63</sup>D. Brust and L. Liu, *Phys. Rev.* **154**, 647 (1967).
- <sup>64</sup>See Table IX of Ref. 9.
- <sup>65</sup>See the review paper by D. E. Aspnes and N. Bottka, in Ref. 3, p. 457.
- <sup>66</sup>J. S. Kline, F. H. Pollak, and M. Cardona, *Helv. Phys. Acta* **41**, 968 (1968).
- <sup>67</sup>J. A. Van Vechten, *Phys. Rev.* **187**, 1007 (1969).
- <sup>68</sup>E. O. Kane, *Phys. Rev. B* **4**, 1910 (1971).
- <sup>69</sup>J. P. Van Dyke, *Phys. Rev. B* **5**, 1489 (1972).